Published in final edited form as:

Proteins. 2017 April ; 85(4): 731–740. doi:10.1002/prot.25252.

Multiple helical conformations of the helix-turn-helix region revealed by NOE-restrained MD simulations of tryptophan aporepressor, TrpR

Balasubramanian Harish[1], **G.V.T. Swapna**[2], **Gregory J. Kornhaber**[2], **Gaetano T. Montelione**[2], and **Jannette Carey**[1,*]

[1]Chemistry Department, Princeton University, Princeton, NJ 08544

[2]Center for Advanced Biotechnology and Medicine, Department of Molecular Biology and Biochemistry, and Northeast Structural Genomics Consortium, Rutgers, The State University of New Jersey, Piscataway, NJ 08854

Abstract

The nature of flexibility in the helix-turn-helix region of *E. coli* trp aporepressor has been unexplained for a long time. The original ensemble of NMR structures showed apparent disorder, but chemical shift and relaxation measurements indicated a helical region. NOE data for a temperature-sensitive mutant showed more helical character in its helix-turn-helix region but nevertheless also led to an apparently disordered ensemble. However, conventional NMR structure determination methods require all structures in the ensemble to be consistent with each NOE simultaneously. The present work uses an alternative approach in which some structures of the ensemble are allowed to violate some NOEs to allow modelling of multiple conformational states that are in dynamic equilibrium. Newly measured NOE data for wild-type aporepressor are used as time-averaged distance restraints in MD simulations to generate an ensemble of helical conformations that is more consistent with the observed NMR data than the apparent disorder in the previously reported NMR structures. The results are consistent with the presence of alternating helical conformations that provide a better explanation for the flexibility of the helix-turn-helix region of trp aporepressor.

Keywords

NMR structure calculation; time-averaging; conformational dynamics; apparent disorder

Introduction

The *E. coli* protein tryptophan repressor (TrpR) is a classic example of a feedback system in which the intracellular concentration of L-tryptophan (L-trp) is self-regulated. Binding of L-trp to the aporepressor enhances affinity and specificity to operator DNA, leading to down-regulation of the expression of genes involved in L-trp biosynthesis[1]. TrpR is a symmetric all-helical dimer (Figure 1A) containing two L-trp binding sites[2]. Helices A, B, C, and F

*Correspondence to: Jannette Carey, Chemistry Department, Princeton University, Princeton, NJ, USA 08544. jcarey@princeton.edu.

from each subunit intertwine to form the hydrophobic core of the dimer, and helices D and E of each subunit form flexible helix-turn-helix (HtH) motifs that contact DNA (Figure 1A). Residues from both subunits participate in each L-trp binding site, yet the binding of L-trp to the aporepressor is not cooperative[3,4]. The absence of cooperativity in L-trp binding despite the dynamics of its proximate HtH motifs may test the suggestion that allostery is an intrinsic property of all dynamic proteins[5].

The HtH region of apoTrpR has been found to exhibit very unusual dynamics in NMR studies[6]. Compared to the central core, the HtH region is observed to be more flexible as indicated by much faster backbone amide proton exchange rates[7] and fewer observed NOEs[8,9]. Nevertheless, relaxation measurements and chemical shift data indicate helical character for the HtH region[9,10]. The conclusion from a large body of work by Jardetzky and co-workers[8–14] is that the HtH region is helical on a nanosecond timescale, but not on a millisecond timescale. A study of apoTrpR backbone amide proton exchange[12] revealed that the intrinsic amide proton exchange rate of the exchanging state differs from a random-coil polypeptide chain. Thus, a two-state equilibrium model between a rapidly exchanging, fully solvent-exposed state and a non-exchanging state is inadequate to explain the data. A helix-coil transition was ruled out, leaving only the unsatisfying explanation that the HtH region is flexible.

To exploit the expected potential of temperature-sensitive mutants to shed light on protein dynamics, a genetic screen was carried out to identify TrpR mutants with lower repression activity at 42°C than at 37°C in presence of the L-trp analogue 5-methyltryptophan[15]. One mutation responsible for the temperature-sensitive phenotype was identified as a change from Leu to Phe of residue 75 at the C-terminus of helix D. This point mutation causes only a slight decrease in affinity for L-trp or DNA, but has a profound effect on the long-range dynamics of apoTrpR[15]. Compared to wild-type (WT) apoTrpR, apoL75F shows higher helical content, but has similar thermal stability. Whereas NOEs revealed a more locally ordered HtH region[16], the NMR structure ensemble of apoL75F (PDB ID: 2XDI) is very similar to WT apoTrpR, and likewise apparently disordered in the HtH region.

Recently, a new crystal structure of temperature-sensitive mutant apoL75F (PDB ID: 3SSX) revealed a distorted conformation in the HtH region on one subunit of the dimer (Figure 1B). The other subunit is in WT conformation, as are both subunits in isomorphous WT apoTrpR crystals[17]. In the distorted conformation, helix D undergoes a rigid-body shift of 3 Å relative to the WT conformation; residues 76–79 in the D-E turn form a 3_{10} helix; and helix E has a local interruption with residues 85–88 looping out. Crystal lattice contacts support the WT-like conformation in one subunit, whereas the distorted conformation in the other subunit lacks crystal contacts, indicating that the mutation is the probable cause of the distortion. The finding that the distorted conformation is not likely to be an artefact of crystallization suggests that this conformation might be present in solution. To evaluate this possibility, NOE data for apoL75F[16] were re-analyzed[17], uncovering evidence for the presence in solution of both the conformations observed in the L75F crystal structure. That finding highlighted a major limitation of current NMR structure determination methods, which neglect conformational dynamics by requiring every structure in the ensemble to be consistent with all NOEs. Under this requirement a single conformer that best fits the data

may not correspond to any actual structure present in the ensemble, and interconversion among multiple ordered conformations can appear as apparent disorder, as observed in the HtH conformations of both WT[9] and L75F[9,16] apoTrpR NMR structures.

The apparent disorder in the NMR structures of WT and L75F apoTrpR may reflect the way NOEs are treated in the molecular dynamics (MD) simulations that are currently used to refine structure models based on NMR data. Distances derived from NOE intensities are treated as upper limits in MD simulations. A penalty is incurred whenever an inter-atomic distance in a modelled structure exceeds its NOE distance limit during the simulation. This penalty is typically applied instantaneously, i.e. the instant a distance exceeds its NOE upper limit. Hence, this approach demands that the structure ensemble satisfy every NOE upper limit continuously during the simulation. To modulate this requirement, van Gunsteren has suggested an alternative method to calculate the penalty function[18] that uses average distances over a specified time period. If an NOE violation occurs, the penalty is not incurred instantly, but only when the time-averaged distance exceeds the NOE upper limit. This 'time-averaging' method allows a structure to transition to conformations that may violate some NOE upper limits. Thus, the ensemble of structures generated from such a simulation might contain members that have violated some NOEs.

This alternative approach of time-averaging is applied in the present work in an effort to clarify the puzzling dynamics of WT TrpR. All the early NMR work on WT TrpR predates the existence of an open-access data repository. The original data could not be recovered from any of the participants in that work. Thus, new NMR data were collected on WT apoTrpR to assign chemical shifts and NOEs. The NMR work, including preparation of the required isotope-enriched protein samples, was accomplished as a Community Outreach Project within the NIH Protein Structure Initiative program.

Methods

Protein preparation

A codon-enhanced gene (for *E. coli* expression) corresponding to full-length WT TrpR was synthesized and the product cloned into a modified NESG_pET15 T7 expression vector encoding an N-terminal His_6 affinity tag and tobacco etch virus protease cleavage site[19]. The final sequence preceding Ala2 of the native TrpR polypeptide is thus MGHHHHHHENLYFQSH. BL21 (λDE3) competent cells were transformed with the resulting construct and expressed in 1 L of uniformly ^{15}N,^{13}C-enriched MJ9 media[20] as follows. A shake-flask culture was grown to mid-log phase at 37 °C (0.5–1.0 OD600 units). Then the culture was shifted to 17 °C and expression induced with 1 mM IPTG. After a period of approximately 16 hours the cell pellet was harvested by centrifugation. The cell pellet was suspended in binding buffer (50 mM Tris-HCl pH 7.5, 500 mM NaCl, 40 mM imidazole) and disrupted by sonication (Misonix 3000). The cleared lysate was subject to Ni-Affinity chromatography (HisTrap HP) and the eluate analyzed by SDS-PAGE. Pooled product was dialyzed at 4 °C overnight and simultaneously treated with TEV protease (1:20, ratio of TrpR to TEV). The sample was then subjected to a subtractive Ni-Affinity step to remove His-tagged components. The flow-through fraction was passed over a gel filtration column (HiLoad 26/60 Superdex 200) equilibrated in NMR buffer (10 mM Tris-HCl buffer

pH 5.7, 100 mM NaCl, 5 mM DTT and 0.02 % NaN_3). Mass spectrometry and SDS-PAGE confirmed that the purification resulted in a highly pure (>95%) uniformly ^{15}N,^{13}C-labeled sample (7 mg yield).

NMR

NMR experiments used uniformly ^{15}N and ^{13}C-enriched apoTpR in 10 mM Tris-HCl buffer pH 5.7 and containing 100 mM NaCl, 5 mM DTT and 0.02 % NaN_3. All NMR spectra were acquired at 40 °C on a Bruker 800 MHz spectrometer. The NMR experiments conducted were: 2D [^1H-^{15}N]-TROSY-HSQC and [^1H-^{13}C]-CH-HSQC; and 3D HNCO, HNCA, HN(CO)CA, HNCACB, CBCA(CO)NH, HBHA(CO)NH, CCH-TOCSY, ^{13}C-edited NOESY and ^{15}N-edited NOESY. The acquisition parameters of each NMR experiment are listed in Supplementary Table S1. The programs NMRPipe[21] and Sparky[22] were used for data processing, peak picking, and resonance assignments. A complete list of backbone and sidechain assignments is given in Supplementary Table S2 and has been deposited in BioMagResDataBase with ID 26821.

NOE analysis

NOE cross-peaks were classified into four categories and assigned distance ranges based on cross-peak intensity: strong (1.8 Å to 3.0 Å), medium (1.8 Å to 4.0 Å), weak (1.8 Å to 5.0 Å), and very weak (1.8 Å to 6.0 Å), with 0.5 Å added to the upper limits for ambiguity of chemically equivalent protons. For comparison with structure models, hydrogen atoms were added to the crystal structure of WT and L75F apoTrpR structures (PDB IDs 3SSW and 3SSX respectively) using the Molprobity server[23]. Each proton-proton distance was measured and compared to the cutoff distance assigned on the basis of the strength of each NOE using a Perl script.

MD simulations

The starting structure of WT apoTrpR in WT conformation was prepared from the 1.1 Å crystal structure PDB ID 3SSW[17], the highest resolution crystal structure of apoTrpR available. Using symmetry operations in YASARA[24] the subunits of the crystal were made to have identical conformations. N-terminal residues 2–5 and C-terminal residues 106–108 that are unresolved in the crystal structure were added to the structure; all residues except the termini (residues 2 and 108) were added in helical conformation and the termini were added in extended conformation. The starting structure of WT apoTrpR in distorted conformation was generated from the subunit with distorted conformation in apo L75F crystal structure PDB ID 3SSX[17] by mutating Phe75 to Leu *in silico* and adding missing residues 1–4 and 107–108 in YASARA[24].

The subsequent steps were all carried out in Gromacs 4.6.5[25,26]. The structure was processed using the AMBER99SB-ILDN force field[27] and placed in a simulation box with periodic boundary conditions for 1 nm beyond the protein. The system was immersed in solvent using a TIP3P water model[28] and six Na^+ ions were added to neutralize the system. Following steepest-descent minimization, each system was further equilibrated in two phases, first for 100 ps in the canonical (NVT) ensemble and second for 100 ps in the

isobaric-isothermal (NPT) ensemble. Both these steps were carried out for solvent relaxation while the protein was kept restrained.

Production run simulations were performed using periodic boundary conditions. The equations of motion were integrated using the leap-frog algorithm[29] with a time step of 2 fs, and the centre-of-mass translation was removed every 1 ps. Bond lengths were constrained using the LINCS algorithm[30]. The temperature and pressure were maintained at 300 K and 1 bar using the Berendsen thermostat with a coupling time of 0.1 ps and barostat with a coupling time of 0.1 ps and isothermal compressibility of 4.5×10^{-5} bar^{-1}. Electrostatics were evaluated using the particle-mesh Ewald method[31] with a cutoff of 10 Å. van der Waals forces were evaluated with a Lennard-Jones potential having a 12 Å cutoff. For time-averaging of NOE restraints[18] the time constant was set to 20 ps and the force constant for the distance restraint was set to 5000 kJ/nm^2.

Trajectories were plotted using the software Plot2, and graphical images were created using Pymol[32].

Accessible surface area calculations

Calculations of accessible surface area were done with the program NACCESS[33], using a water molecule of 1.4 A radius as solvent probe and a slice size of 0.05 Å.

Results and Discussion

NMR data for WT TrpR

The 2D [^{1}H-^{15}N]-TROSY-HSQC spectrum of WT apoTrpR (Figure 2) shows prominent differences from previously reported results. Cross-peaks assigned to the amides of Met42, Thr44, Arg84 and Gly85 are observed here, but had been reported as missing from the WT apoTrpR spectrum in the most recent work[16]. That work considered the absence of these four cross-peaks in the WT spectrum, and their presence in the L75F spectrum, as reflecting a difference in dynamics between WT and L75F. However, comparison with other earlier reports[8,34] establishes that these cross-peaks had likely been observed in WT TrpR in the older NMR studies, because ^{1}H and ^{15}N chemical shifts for each of these residues were assigned in those studies. Thus, only in the 2002 work[16] are these four cross-peaks absent. As will be shown here, these [^{1}H-^{15}N]-TROSY-HSQC cross-peaks arise from residues directly involved in a conformational transition in WT TrpR.

NMR spectra from 2D and 3D heteronuclear NMR experiments were used to assign the backbone and sidechain resonances of WT apoTrpR. Of the 103 non-proline residues in each monomer, 96 ^{1}H-^{15}N amides could be assigned unambiguously. Additionally, 102 Cα resonances were also assigned. A complete list of backbone and sidechain assignments is given in Supplementary Table S2 and has been deposited in the BioMagResDB (BMRB ID 26821). Consistent with previous results[9], the Cα and Hα chemical shift ranges indicate helical character in the D–E regions, based on comparison with random-coil chemical shifts[35].

NOEs were assigned from ^{15}N-edited and ^{13}C-edited ^{1}H-^{1}H NOESY spectra. Of 1182 identified cross-peaks, 710 unique NOE intensities were used to derive upper distance limits between the corresponding protons, using the procedure outlined by Jardetzky and co-workers (see Methods)[9]. Compared to core helices A, B, C, and F, the D and E helices comprising the HtH motif show fewer of the i,i+3 and i,i+4 NOE connectivities between backbone amide and alpha protons that are characteristic of helical segments. However, many of the observed NOEs (see Supplementary Table 2) are consistent with helical structures, as was also noted in earlier work[9].

NOE data analysis

The previously reported NMR structure of WT apoTrpR[9], which treated NOE distances as instantaneous restraints, shows apparent disorder in the HtH region, as the observed NOEs are not consistent with a single helical model. To evaluate whether conformations similar to the two observed in the crystal structure of dimeric apoL75F TrpR are consistent with the NOE data collected for WT apoTrpR in the present work, a detailed comparison was made between the experimental NOE distance limits and two specific structural models of the HtH region based on those crystal conformations. The evaluation used the WT conformation from the WT apoTrpR crystal structure (PDB ID 3SSW) and a hypothetical distorted conformation of WT apoTrpR prepared by creating a symmetric dimer from the distorted subunit of the L75F crystal structure (PDB ID 3SSX) and mutating Phe75 back to the WT residue Leu *in silico.* Twelve of the measured NOE intensities are inconsistent with the inter-proton distances calculated for these two models, indicating a conflict with one or both conformations (Table 1).

Of the twelve conflicting NOEs, four are consistent with the distorted conformation, but not with the WT conformation. All four of these NOEs involve residues 75–79, which form a 3_{10} helix in the distorted subunit of the L75F TrpR crystal structure. These four conflicting NOEs are consistent with the distances in a 3_{10} helix, suggesting that the 3_{10} helix observed in the L75F crystal structure might also be present within the ensemble of WT apoTrpR conformations in solution. Three other NOEs are consistent with the WT conformation but not with the distorted conformation. One of these NOEs involves a long-range contact between the sidechains of Ile57 and Thr81, consistent with the tertiary packing of helix C with helix E in the WT conformation. Finally, five NOEs are not consistent with either conformation, suggesting the presence of additional conformations in solution. Thus, the NOE data suggest the presence of both WT and distorted conformations in WT apoTrpR, and they also indicate the presence of additional conformations.

MD simulations

To explore the conformational landscape of WT apoTpR, MD simulations were performed starting from symmetrized structures in which both subunits had either WT or distorted HtH conformations. These simulations used the WT apoTpR NOE data determined in the present work as time-averaged distance restraints[18]. Two representative inter-proton distances shown in Figure 3 trace the trajectories of the simulations. One of these, the observed NOE between one pair of protons (I57Hγ2 and T81Hγ2, reflecting the tertiary contact described above) is consistent with the WT conformation only, and the other, the NOE between the second

proton pair (G76H and I79Hβ, reflecting the 3_{10} helix described above) is consistent with the distorted conformation only.

The trajectory of a 20 ns simulation of the WT apoTrpR dimer starting with WT HtH conformations in both subunits shows dramatically different behaviour in the two subunits. In the initial WT conformation both subunits have I57Hγ2-T81Hγ2 distances below the NOE upper bound (Figure 3A) and G76H-I79Hβ distances above the NOE upper bound (Figure 3B). In one subunit the I57Hγ2-T81Hγ2 distance remains below the NOE upper bound throughout the simulation and the G76H-I79Hβ distance remains above the upper bound; thus this subunit remains in the WT conformation (red line in Figure 3A,B). In the other subunit the G76H-I79Hβ distance (blue line in Figure 3B) moves below the NOE upper bound early in the simulation (~0.1 ns), while the I57Hγ2-T81Hγ2 distance (blue line in Figure 3B) fluctuates above and below the upper bound until ~5 ns, after which the I57Hγ2-T81Hγ2 distance is consistently above the upper bound. Snapshots from the trajectory (Figure 4A) show that this subunit is in the distorted conformation after 5 ns.

Simulation of WT apoTrpR starting with distorted HtH conformations in both subunits again shows different behaviour in the two subunits. Neither subunit samples the WT conformation; they violate the I57Hγ2-T81Hγ2 NOE upper bound throughout the simulation (Figure 3C,D). However, one subunit (green line in Figure 3C,D) also violates the upper bound of G76H-I79Hβ, indicating that this subunit is not in the distorted conformation. A snapshot of this subunit at 15 ns in the simulation (Figure 4) shows that the D–E loop resembles the WT conformation, but the interruption in helix E persists as in the distorted conformation. This result indicates the presence of a structure intermediate between the WT and distorted conformations.

Further analysis of the trajectories was done by inspecting the time course of inter-proton distances corresponding to NOEs that are inconsistent with both WT and distorted conformations (Supplementary Figure S1). Two inter-proton distances (G76H-I79Hγ1 and N87H-L89Hδ1) are below the NOE upper bounds during the transition from WT to distorted conformation, suggesting a transient population of an intermediate conformation. However, none of the other conformations sampled in either simulation show interproton distances that could account for the remaining three NOEs. This result might reflect the fact that the simulations sample only a small portion of the time scale of molecular motions.

To summarize, a conformational transition from WT to distorted conformation is observed in MD simulation of WT apoTrpR, but the reverse conformational transition is not observed in simulation of distorted apoTrpR. Although the numbers of NOE violations in the WT and distorted conformations are nearly the same, the magnitudes of the violations are larger in the WT conformation than in the distorted conformation (Table 1). This means that the simulation starting in the WT conformation incurs larger penalties, and these might favour a conformational transition. In comparison, simulation starting from the distorted conformation incurs relatively lower penalties, consistent with more minor structural fluctuations.

Discussion

The results presented here support the view[18] that using NOEs as time-averaged restraints can be important for dynamic systems. The previously reported NMR structure for WT apoTrpR[9], which did not allow for NOE violations, showed no helical conformations in the HtH region. Thus, the calculated structure models had in fact lost valuable information contained in the NOEs and chemical shift data, and did not accurately reflect the dynamics of the HtH region, a point acknowledged by the authors of the original work[9]. In contrast, the structure ensembles generated by time-averaging of NOE restraints in the present work are consistent with the previously reported chemical shift data[9] and backbone amide exchange rates[14]. The present results also indicate that discrete helical conformations, and not apparent disorder, underlie HtH flexibility in TrpR.

Nevertheless, the use of NOEs as time-averaged distance restraints can provide only a list of conformations consistent with the data. Whereas some NMR parameters like chemical shifts and coupling constants are ensemble-averages with contributions from all members of the ensemble, NOEs are not averaged over all conformations[36] and may over-represent transitory close encounters. Hence NOEs cannot be used to quantify the populations of different conformations or the rates of their interconversion. Additional lines of evidence like chemical shift data[9] indicating an overall helical region provide further support for the presence of both WT and distorted conformations in the WT apoTrpR ensemble.

Although the NOE data do not quantify conformer populations, the relative populations of conformers can be estimated based on earlier work. The association and dissociation rates for L-trp—TrpR binding[13] have been determined to be 9.9×10^6 M^{-1} s^{-1} and 2.0×10^3 s^{-1}, respectively. The diffusion-controlled association rate for this reaction is calculated to be 2.6×10^7 M^{-1} s^{-1} using the Smoluchowski equation[37] and the estimated sizes and diffusion coefficients[38] of the protein and ligand. The fact that the experimentally determined association rate is slower than the diffusion-limited expectation value is interpreted to reflect the presence of one or more protein conformations that are incompatible with L-trp binding. The ratio of the two rates is then a reflection of the relative populations of binding-compatible and binding-incompatible conformations. The equilibrium ratio of binding-compatible and binding-incompatible conformations is thus ~2.6:1. Assuming that only the WT conformation is binding-compatible (an untested assumption), this result corresponds to approximately ~72% of apoTrpR in the WT conformation in solution at equilibrium. The data do not resolve how much of the remaining 28% is represented by the distorted conformer and how much by other transient conformational states.

The presence of the distorted conformation in apoTrpR has relevance for the mechanism of L-trp binding. The distorted conformation is presumably incompatible with L-trp binding because Ile82 occludes the binding site for L-trp[17]. L-trp binding to apoTrpR is accompanied by a large negative ΔC_p of −460 cal $mol^{-1}K^{-1}$ (ref.[4]). Conventionally, the magnitude of ΔC_p has been correlated with changes in accessible surface area (ASA) in ligand binding, ascribed largely to the hydrophobic effect[39]. Model studies[40,41] have parameterized the heat capacity contributions of polar and non-polar surface area changes. Those values suggest that only a change in ASA corresponding to a complete disorder-order

transition of the HtH region could account for the experimental ΔC_p[4], although NMR data ruled out such a disorder-order transition[6,9]. The present results allow the calculation of ΔC_p values based on the difference in ASA between distorted and WT conformations in apoTrpR (see Methods), yielding ΔC_p −225.2 cal $mol^{-1}K^{-1}$ using the values of Murphy et al.[40] and ΔC_p −169.2 cal $mol^{-1}K^{-1}$ using the values of Spolar et al.[41], both of which are much smaller than the measured ΔCp.

The inability of the hydrophobic effect to fully account for the observed ΔCp values has been found in many systems[42–46]. These 'anomalous' ΔC_p values have been rationalized in many ways: by sequestered water molecules[47,48], hydrogen bonding[49], and other cooperative weak interactions[50]. However, as pointed out by Cooper[51], ΔC_p values observed in protein folding and ligand binding are comparable to the values for similar processes in small molecules and thus are not really anomalous. In this view, the large heat capacities of ligand binding are attributed not just to the hydrophobic effect, but also involve contributions from changes in conformational dynamics and other intramolecular interactions. However, current empirical models are still inadequate in providing a quantitative interpretation of heat capacity values.

The present results shed light on an intriguing aspect of ligand binding to dimeric TrpR, the absence of cooperativity between the two L-trp binding events[3,4]. Thus TrpR presents an exception to the proposal that allostery may be a feature of all dynamic ligand-binding proteins[5]. The MD simulations in this work suggest a possible explanation for this result[4]. Irrespective of the starting structure and any transitions that occur during the simulations, the HtH regions show much higher fluctuations compared to the dimer core (Figure 5). Fluctuations in the HtH region do not propagate into the core beyond residue ~60 near the centre of helix C. Even the transition in one subunit from WT to distorted HtH conformation does not affect the other HtH, which remains in WT conformation. These findings suggest that L-trp binding at one site does not affect dynamics at the other HtH region, explaining why the affinity at the second site remains unaltered. Thus, the present results suggest that confinement of dynamics may suppress allostery. An interesting question for future work is exactly how the intervening dimeric core of TrpR impedes signal transmission between the binding sites.

Supplementary Material

Refer to Web version on PubMed Central for supplementary material.

Acknowledgments

This work was supported by grant DBI10-04830 from NSF to J.C. and grants U54 GM094597 and 1S10-OD018207 from NIH to G.T.M. This work utilized the services of TIGRESS, a high-performance computing center that is supported jointly by the Research Computing Department of the Princeton University Office of Information Technology and the Princeton Institute for Computational Science and Engineering. B.H. and J.C. express their gratitude for the advice and hospitality of colleagues at Lund University, Sweden, and the Czech Academy of Sciences at Nové Hrady.

References

1. Rose JK, Squires CL, Yanofsky C, Yang HL, Zubay G. Regulation of in vitro transcription of the tryptophan operon by purified RNA polymerase in the presence of partially purified repressor and tryptophan. Nature New Biol. 1973; 245:133–137. [PubMed: 4582892]
2. Schevitz RW, Otwinowski Z, Joachimiak A, Lawson CL, Sigler PB. The three-dimensional structure of trp repressor. Nature. 1985; 317:782–786. [PubMed: 3903514]
3. Arvidson DN, Bruce C, Gunsalus RP. Interaction of the Escherichia coli trp aporepressor with its ligand, L-tryptophan. J Biol Chem. 1986; 261:238–243. [PubMed: 3079755]
4. Jin L, Yang J, Carey J. Thermodynamics of ligand binding to trp repressor. Biochemistry. 1993; 32:7302–7309. [PubMed: 8343520]
5. Gunasekaran K, Ma B, Nussinov R. Is allostery an intrinsic property of all dynamic proteins? Proteins. 2004; 57:433–443. [PubMed: 15382234]
6. Gryk, MR., Jardetzky, O. Flexibility and function of the Escherichia coli trp repressor. In: Markley, JL., Opella, SJ., editors. Biological NMR Spectroscopy. 1997. p. 29-49.
7. Czaplicki J, Arrowsmith C, Jardetzky O. Segmental differences in the stability of the trp-repressor peptide backbone. J Biomol NMR. 1991; 1:349–361. [PubMed: 1841704]
8. Arrowsmith C, Pachter R, Altman R, Jardetzky O. The solution structures of Escherichia coli trp repressor and trp aporepressor at an intermediate resolution. Eur J Biochem. 1991; 202:53–66. [PubMed: 1935980]
9. Zhao D, Arrowsmith CH, Jia X, Jardetzky O. Refined solution structures of the Escherichia coli trp holo- and aporepressor. J Mol Biol. 1993; 229:735–746. [PubMed: 8433368]
10. Zheng Z, Czaplicki J, Jardetzky O. Backbone dynamics of trp repressor studied by 15N NMR relaxation. Biochemistry. 1995; 34:5212–5223. [PubMed: 7711041]
11. Arrowsmith CH, Czaplicki J, Iyer SB, Jardetzky O. Unusual dynamic features of the trp repressor from Escherichia coli. J Am Chem Soc. 1991; 113:4020–4022.
12. Finucane MD, Jardetzky O. Mechanism of hydrogen-deuterium exchange in trp repressor studied by 1H-15N NMR. J Mol Biol. 1995; 253:576–589. [PubMed: 7473735]
13. Schmitt TH, Zheng Z, Jardetzky O. Dynamics of tryptophan binding to Escherichia coli Trp repressor wild type and AV77 mutant: an NMR study. Biochemistry. 1995; 34:13183–13189. [PubMed: 7548081]
14. Gryk MR, Finucane MD, Zheng Z, Jardetzky O. Solution dynamics of the trp repressor: a study of amide proton exchange by T1 relaxation. J Mol Biol. 1995; 246:618–627. [PubMed: 7877180]
15. Jin L, Fukayama JW, Pelczer I, Carey J. Long-range effects on dynamics in a temperature-sensitive mutant of trp repressor. J Mol Biol. 1999; 285:361–378. [PubMed: 9878412]
16. Tyler R, Pelczer I, Carey J, Copié V. Three-dimensional solution NMR structure of Apo-L75F-TrpR, a temperature-sensitive mutant of the tryptophan repressor protein. Biochemistry. 2002; 41:11954–11962. [PubMed: 12356295]
17. Carey J, Benoff B, Harish B, Yuan L, Lawson CL. Environment-dependent long-range structural distortion in a temperature-sensitive point mutant. Protein Sci. 2012; 21:63–74. [PubMed: 22057811]
18. Torda AE, Scheek RM, van Gunsteren WF. Time-averaged nuclear Overhauser effect distance restraints applied to tendamistat. J Mol Biol. 1990; 214:223–235. [PubMed: 2370663]
19. Acton TB, Xiao R, Anderson S, Aramini J, Buchwald WA, Ciccosanti C, Conover K, Everett J, Hamilton K, Huang YJ, et al. Preparation of Protein Samples for Nmr Structure, Function, and Small-Molecule Screening Studies. Meth Enzymol. 2011; 493:21–60. [PubMed: 21371586]
20. Jansson M, Li Y-C, Jendeberg L, Anderson S, Montelione G, Nilsson BR. High-level production of uniformly ^{15}N-and ^{13}C-enriched fusion proteins in Escherichia coli. J Biomol NMR. 1996; 7:131–141. [PubMed: 8616269]
21. Delaglio F, Grzesiek S, Vuister GW, Zhu G, Pfeifer J, Bax A. NMRPipe: a multidimensional spectral processing system based on UNIX pipes. J Biomol NMR. 1995; 6:277–293. [PubMed: 8520220]
22. Goddard TD, Kneller DG. SPARKY 3.

23. Chen VB, Arendall WB, Headd JJ, Keedy DA, Immormino RM, Kapral GJ, Murray LW, Richardson JS, Richardson DC. MolProbity: all-atom structure validation for macromolecular crystallography. Acta Crystallogr D Biol Crystallogr. 2010; 66:12–21. [PubMed: 20057044]
24. Krieger E, Koraimann G, Vriend G. Increasing the precision of comparative models with YASARA NOVA–a self-parameterizing force field. Proteins. 2002; 47:393–402. [PubMed: 11948792]
25. Berendsen H, van der Spoel D, van Drunen R. Gromacs - a Message-Passing Parallel Molecular-Dynamics Implementation. Computer Physics Communications. 1995; 91:43–56.
26. Pronk S, Páll S, Schulz R, Larsson P, Bjelkmar P, Apostolov R, Shirts MR, Smith JC, Kasson PM, van der Spoel D, et al. GROMACS 4.5: a high-throughput and highly parallel open source molecular simulation toolkit. Bioinformatics. 2013; 29:845–854. [PubMed: 23407358]
27. Lindorff-Larsen K, Piana S, Palmo K, Maragakis P, Klepeis JL, Dror RO, Shaw DE. Improved side-chain torsion potentials for the Amber ff99SB protein force field. Proteins. 2010; 78:1950–1958. [PubMed: 20408171]
28. Berendsen, H., Postma, J., van Gunsteren, WF., Hermans, J. Interaction models for water in relation to protein hydration. In: Pullman, B., editor. Intermolecular Forces. 1981. p. 331-342.
29. van Gunsteren WF, Berendsen HJC. A Leap-frog Algorithm for Stochastic Dynamics. Molecular Simulation. 1988; 1:173–185.
30. Hess B, Bekker H, Berendsen HJC, Fraaije GEM. LINCS: a linear constraint solver for molecular simulations. J Comput Chem. 1997; 18:1463–1472.
31. Essmann U, Perera L, Berkowitz ML, Darden T, Lee H, Pedersen LG. A smooth particle mesh Ewald method. J Chem Phys. 1995; 103:8577–8593.
32. Delano WL. The PyMOL Molecular Graphics System. 2002
33. Hubbard S, Thornton JM. NACCESS. 1993
34. Arrowsmith CH, Pachter R, Altman RB, Iyer SB, Jardetzky O. Sequence-specific 1H NMR assignments and secondary structure in solution of Escherichia coli trp repressor. Biochemistry. 1990; 29:6332–6341. [PubMed: 2207078]
35. Wishart DS, Nip AM. Protein chemical shift analysis: a practical guide. Biochem Cell Biol. 1998; 76:153–163. [PubMed: 9923684]
36. Jardetzky O. On the nature of molecular conformations inferred from high-resolution NMR. Biochim Biophys Acta. 1980; 621:227–232. [PubMed: 7353041]
37. Cantor, CR., Schimmel, PR. The Behavior of Biological Macromolecules. W.H. Freeman; 1980. p. 916-922.
38. Joachimiak A, Kelley RL, Gunsalus RP, Yanofsky C, Sigler PB. Purification and characterization of trp aporepressor. Proc Natl Acad Sci USA. 1983; 80:668–672. [PubMed: 6338493]
39. Spolar RS, Record MT. Coupling of local folding to site-specific binding of proteins to DNA. Science. 1994; 263:777–784. [PubMed: 8303294]
40. Murphy KP, Freire E. Thermodynamics of Structural Stability and Cooperative Folding Behavior in Proteins. Adv Protein Chem. 1992; 43:313–361. [PubMed: 1442323]
41. Spolar RS, Livingstone JR, Record MT. Use of liquid hydrocarbon and amide transfer data to estimate contributions to thermodynamic functions of protein folding from the removal of nonpolar and polar surface from water. Biochemistry. 1992; 31:3947–3955. [PubMed: 1567847]
42. Holdgate GA, Tunnicliffe A, Ward WH, Weston SA, Rosenbrock G, Barth PT, Taylor IW, Pauptit RA, Timms D. The entropic penalty of ordered water accounts for weaker binding of the antibiotic novobiocin to a resistant mutant of DNA gyrase: a thermodynamic and crystallographic study. Biochemistry. 1997; 36:9663–9673. [PubMed: 9245398]
43. Bergqvist S, Williams MA, O'Brien R, Ladbury JE. Heat Capacity Effects of Water Molecules and Ions at a Protein-DNA Interface. J Mol Biol. 2004; 336:829–842. [PubMed: 15095863]
44. Bello M, Pérez-Hernández G, Fernández-Velasco DA, Arreguín-Espinosa R, García-Hernández E. Energetics of protein homodimerization: Effects of water sequestering on the formation of β-lactoglobulin dimer. Proteins. 2007; 70:1475–1487.
45. Pineda JRET, Callender R, Schwartz SD. Ligand Binding and Protein Dynamics in Lactate Dehydrogenase. Biophys J. 2007; 93:1474–1483. [PubMed: 17483170]

46. Stegmann CM, Seeliger D, Sheldrick GM, de Groot BL, Wahl MC. The thermodynamic influence of trapped water molecules on a protein-ligand interaction. Angew Chem Int Ed Engl. 2009; 48:5207–5210. [PubMed: 19499554]

47. Habermann SM, Murphy KP. Energetics of hydrogen bonding in proteins: a model compound study. Protein Sci. 1996; 5:1229–1239. [PubMed: 8819156]

48. Cooper A. Heat capacity effects in protein folding and ligand binding: a re-evaluation of the role of water in biomolecular thermodynamics. Biophys Chem. 2005; 115:89–97. [PubMed: 15752588]

49. Cooper A. Heat capacity of hydrogen-bonded networks: an alternative view of protein folding thermodynamics. Biophys Chem. 2000; 85:25–39. [PubMed: 10885396]

50. Cooper A, Johnson CM, Lakey JH, Nöllmann M. Heat does not come in different colours: entropy-enthalpy compensation, free energy windows, quantum confinement, pressure perturbation calorimetry, solvation and the multiple causes of heat capacity effects in biomolecular interactions. Biophys Chem. 2001; 93:215–230. [PubMed: 11804727]

51. Cooper A. Protein Heat Capacity: An Anomaly that Maybe Never Was. J Phys Chem Lett. 2010; 1:3298–3304.

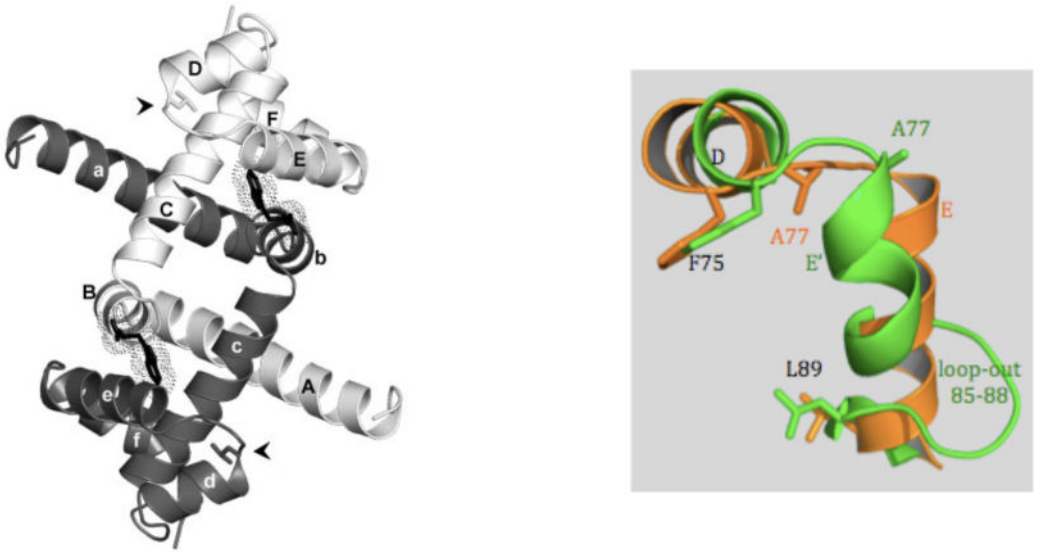

Figure 1. TrpR structures

(A) The WT holoTrpR dimer crystal structure (PDB ID: 2OZ9), showing the arrangement of helices (light subunit: A–F; dark subunit: a–f) and L-tryptophan ligands (black skeletal models and dotted surfaces). Leu 75 (stick model at black arrowheads) lies within the DNA-binding helix-turn-helix region. (B) Overlay of HtH regions from each subunit in the crystal structure of mutant L75F apoTrpR dimer (PDB ID: 3SSX), showing two conformations of helices D and E. Orange, WT-like conformation; green, distorted conformation.

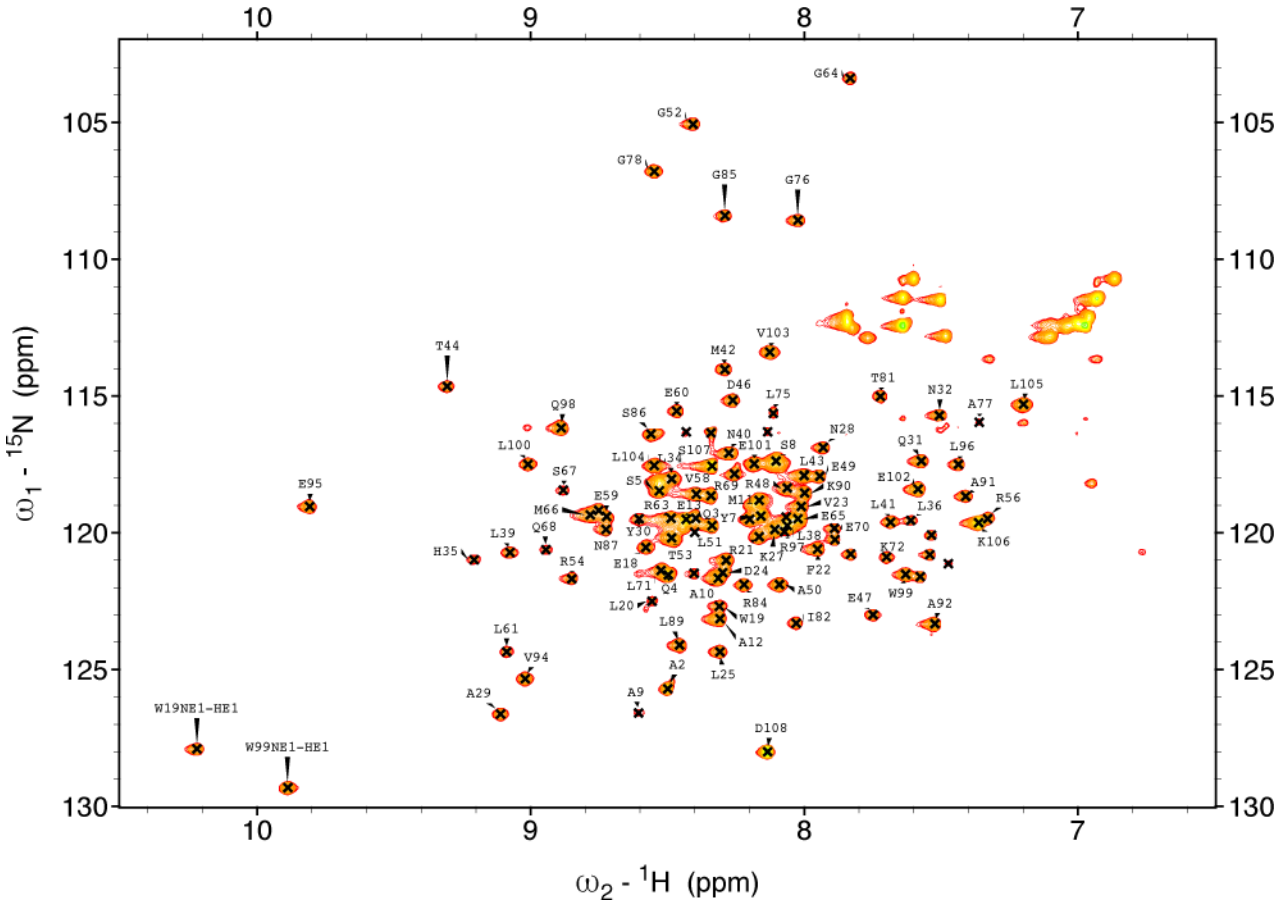

Figure 2. NMR data

^{1}H-^{15}N HSQC spectrum of WT apoTrpR recorded at 40°C in 10 mM Tris-HCl buffer pH 5.7 containing 100 mM NaCl, 5 mM DTT, and 0.02 % NaN3. Unlabelled peaks in the 6.8–8.0 (^{1}H)/110–115 (^{15}N) ppm region are from sidechain –NH_2 groups.

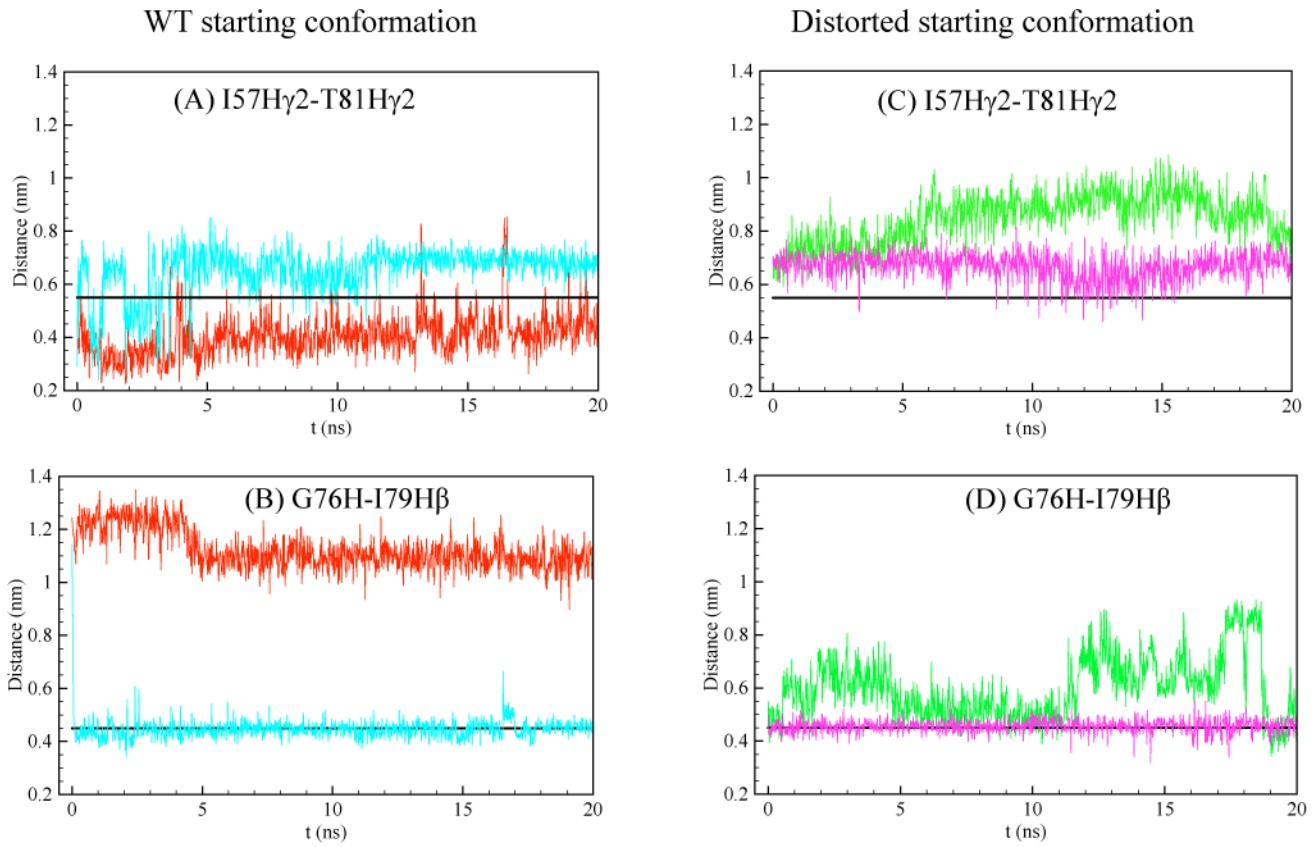

Figure 3. MD simulations

Distance (in nm) between selected protons in each subunit of WT TrpR during simulation starting from WT conformation in both subunits (left, panels A and B) or starting from distorted conformation in both subunits (right, panels C and D). Upper, panels A and C, bond distance between I57Hγ2 and T81Hγ2 atoms; lower, panels B and D, bond distance between G76H and I79Hβ atoms. The two colours in each panel denote the two subunits. The NOE-derived upper distance limit is shown as a black line within each panel.

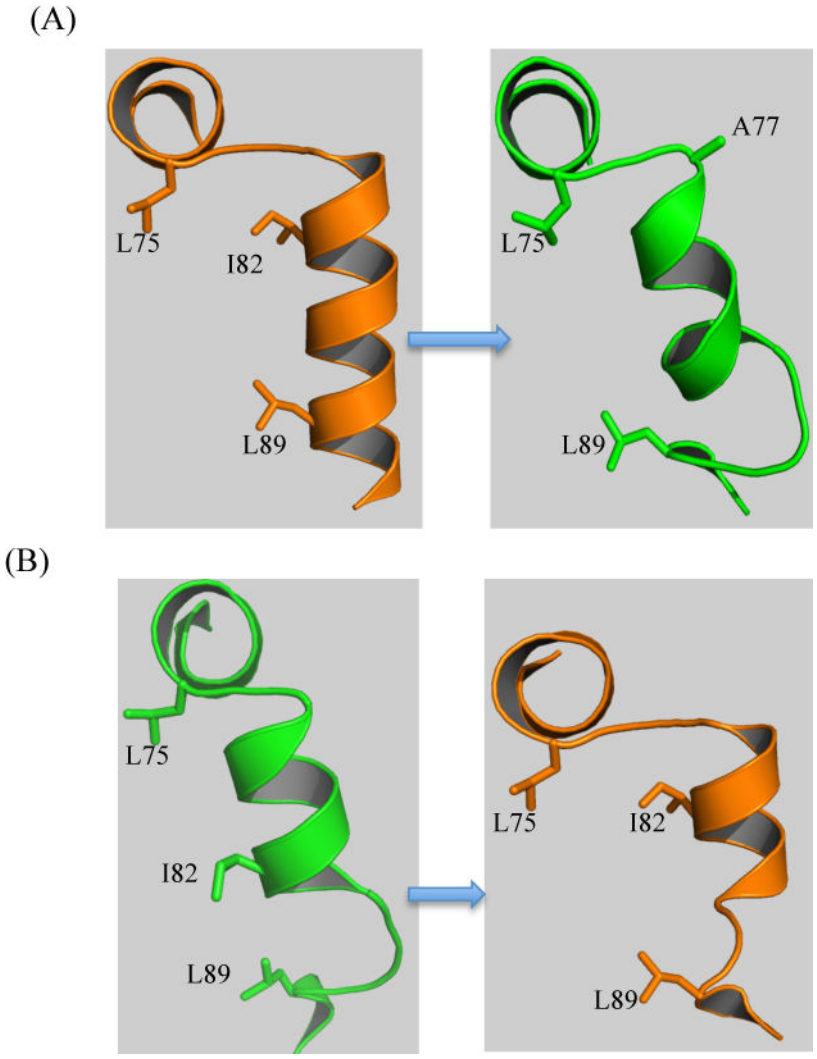

Figure 4. WT apoTrpR conformational transitions

(A) Simulation starting in WT conformation (left, snapshot at 0 ns) and sampling distorted conformation (right, snapshot at 13 ns); (B) Simulation starting in distorted conformation (left, snapshot at 0 ns) and sampling an intermediate conformation (right, snapshot at 15 ns).

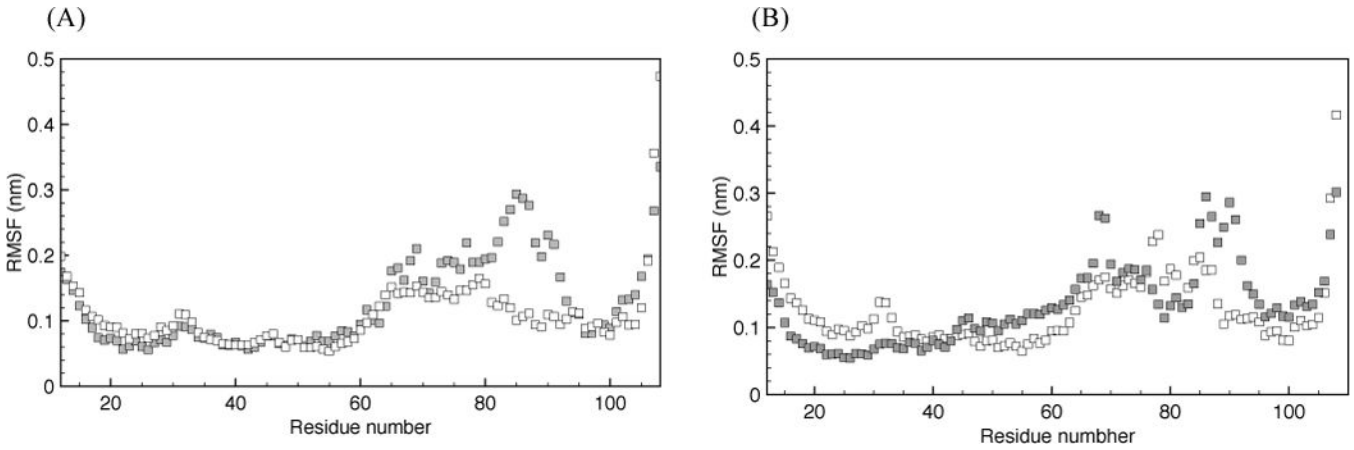

Figure 5. Structure fluctuations

Root mean square fluctuations (RMSF) of backbone atoms of each residue relative to starting structure during 20 ns simulations of WT apoTrpR starting with both subunits in (A) WT conformation or (B) distorted conformation. One subunit is represented by black squares and the other subunit by white squares. Residues 1–11 are omitted because of their high mobility.

Table 1

Comparison of NOEs and interproton distances in apo WT TrpR.

Observed NOEs			apoTrpR crystal structures	
Proton 1	**Proton 2**	**NOE upper-limit distance (Å)**	**WT structure interproton distances (Å)**	**Distorted structure Interproton distances (Å)**
L75Hβ	I79Hδ1	**6.5**	12.6–14.9	**3.3–4.8**
L75H	I79Hβ	**5.0**	12.7	**4.9**
L75Hα	G78H	**5.5**	8.3	**5.4**
G76H	I79Hβ	**4.5**	12.2	**4.5**
G76H	I79Hγ1	5.5	11.0–11.8	6.3–7.0
A77Hβ	I79Hδ	5.5	10.1–12.3	8.5–10.3
A77Hβ	I79H	4.5	6.6–7.9	5.1–5.6
I82H	G85Hα	5.0	5.6–6.9	6.7–8.1
N87H	L89Hδ1	6.5	7.2	8.6
I57Hγ2	T81Hγ2	**5.5**	**3.6–6.6**	6.9–9.8
N87H	L89H	**4.5**	**4.2**	6.8
G78H	T81H	**4.5**	**3.7**	6.0

Interproton distances or distance ranges were measured between predicted hydrogen atom positions in the WT apoTrpR models prepared from WT apoTrpR crystal structure for WT conformation and L75F apoTrpR crystal structure for distorted conformation as explained in Methods.

Bold ranges denote consistency between an NOE and the interproton distance in the indicated crystal structure.